Correlation Analysis of Ultrasonic Stress Wave Characteristics and the Destructive Strength Measurements in Cylindrical Wooden Structure

Yishi Lee, Frederico José Nistal França, R. Daniel Seale, Jerrold E. Winandy, and Christopher A. Senalik

***Abstract*—The utility sector has been employing ultrasonic-based nondestructive evaluation (NDE) to determine the cross-sectional groundline integrity of wooden utility poles. While it is far less invasive than other methods, its efficacy has not been thoroughly studied. This study aims to fill this technical gap by analyzing the correlation between the propagational characteristics of the ultrasonic stress wave using a novel embedded waveguide technique and the existing destructive testing methods. The proposed embedded waveguide technique excites diffusive Rayleigh mode (AW2) propagating in the shell region of the cross-sectional plane. This discovery allows a direct examination of the shell region condition through stress wave analysis. By employing the Gabor wavelet transformation and the model-based arrival region identification, this proposed technique extracts the propagation velocity and the associated spectral response of AW2. This study uses the static break assessment per ASTM 1036 Standard Test Methods And The longitudinal compression test per ASTM D143–14 "secondary method" to quantify the cross-sectional strength of the test specimen. This work performs a comprehensive correlation analysis between the extracted AW2 features and the associated destructive test. An overall correlation R^2 from 0.2 to 0.5 is achieved between the AW2 features and the static break test results. An overall correlation of R^2 of 0.4 is achieved for 30–35 ft poles in the longitudinal compression test.**

***Index Terms*—Industrial measurement and control, material and defect characterization, signal and image processing, wave propagation (including elastic waves), wooden utility poles.**

Manuscript received September 8, 2021; accepted October 8, 2021. Date of publication October 14, 2021; date of current version December 30, 2021. This work was supported in part by the Utility Asset Management Inc. (UAM), Denver, CO, USA, and in part by Mississippi State University (MSU), Mississippi State, MS, USA, for the nondestructive diagnostic instruments and destructive testing equipment. *(Corresponding author: Yishi Lee.)*

Yishi Lee is with the Department of Engineering and Engineering Technology, Metropolitan State University of Denver, Denver, CO 80128 USA (e-mail: ylee24@msudenver.edu).

Frederico José Nistal França and R. Daniel Seale are with the College of Forest Resources, Mississippi State University, Starkville, MS 39762 USA.

Jerrold E. Winandy is with Winandy and Associates LLC, Ham Lake, MN 55304 USA.

Christopher A. Senalik is with the USDA Forest Products Laboratory, Madison, WI 53726 USA.

Digital Object Identifier 10.1109/TUFFC.2021.3120067

I. Introduction

THE United States power and communication infrastructure relies on the structural integrity of approximately 154 million wooden utility poles [1]. A reliable structural monitoring system is vital to ensure the sustainability of these networks. The traditional evaluation process has relied on partial excavation and sound and bore techniques, but the invasive nature can inadvertently damage the internal chemical and physical characteristics. A recent study conducted by Winandy [2] reveals that any incision in the wooden surface could negatively affect the strength in the cross-sectional plane. Additionally, the American National Standards Institute (ANSI) specification for new poles [3] prohibits open or plugged holes. Comparison studies by U.S. utilities have indicated that ultrasonic nondestructive testing (NDT) can produce the same level of efficacy as the partial excavate, sound, and bore process. However, the correlation between ultrasonic NDT and destructive tests has not been quantitatively evaluated. This study aims to explore the statistical relations between the ultrasonic method with the destructive evaluation methods [4], [5].

The challenge of ultrasonic stress waves in wood was first examined by Fukuda [6]. A study conducted by Bucur [7] explored the orthotropic property of elastic propagation in the longitudinal, radial, and tangential directions. The relationship between the attenuation and the elastic moduli was evaluated by Dunlop [8]. A more detailed analysis was later performed by Suzuki *et al.* [9] to examine the grain angle effects on the ultrasonic velocity. The associated theoretical and numerical models have been developed to understand the stress wave propagational mechanism [10]–[12]. Winandy and Morrell [13] evaluated the efficacy of ultrasonic inspection of progressively decayed wood in 1993 and concluded that using time-of-flight (TOF) as a sole metric for wood characterization appeared unreliable. In 1992, Bucur and Feeney [14] pioneered the study of the energy interactions with the dispersive medium. Due to the complex wave interactions within the medium, there are various attempts of extracting features in the received signal to improve the characterization of the physical properties of the medium. That includes time centroid measurements [15], signal attenuation by using root-mean-square

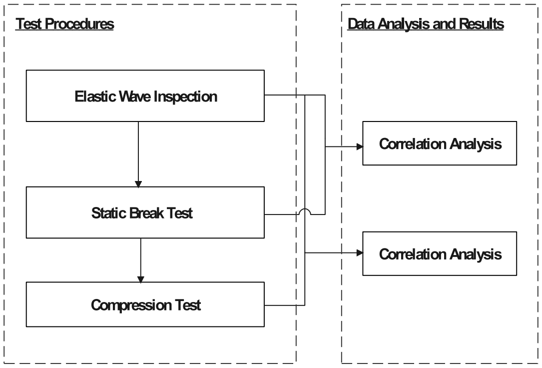

Fig. 1. Sequence of the test and the proposed analysis approach.

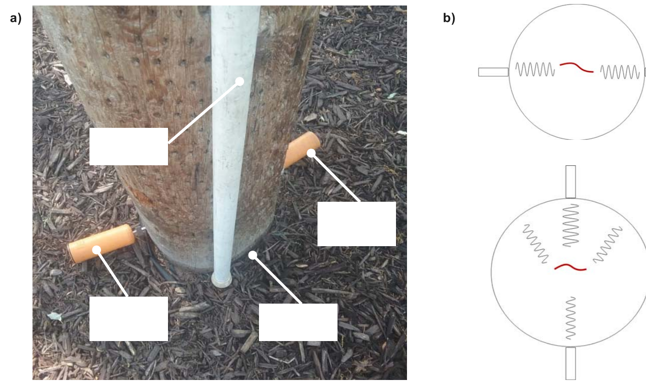

Fig. 2. (a) Ground-line ultrasonic test with UB1000. (b) Orientation of localized defect and plane wave response.

(RMS) [16], and fuzzy logic [17]. Lee [18] and Lee *et al.* [19] incorporated the findings from the elastodynamic formulation into the signal analysis process, effectively uncovers different arrivals within the waveform. Using time–frequency (TF) domain representation, critical parameters of a reflected stress wave can be extracted to characterize the material property. Senalik *et al.* [20] in his recent study performed a thorough analysis by formulating a multivariable linear regression (MLR) as a function of reflected signal parameters and known material properties to estimate the ultimate tensile strength (UTS).

The shell region near the groundline sustains significant cyclic compression and tension stresses from transverse wind loads. Any decay in this region decreases the maximum load more significantly than the heart region decay. Building upon the previous studies, this study focuses on the shell region propagation of the Rayleigh mode excited by the novel embedded waveguide. It began with the ultrasonic test by acquiring the through-transmission stress wave signal using the UB1000 device. The ultrasonic test is performed in the cross-sectional planes from 1 ft below grade up to 4 ft above grades with a 1 ft longitudinal increment. Section II-A discusses the test procedures. The associated physics-based signal analysis technique of extracting vital information from the stress wave signal is explained in Section II-B. The poles are then subjected to the static break test per the ASTM 1036 standard test method. The setup and the system of performing static mechanical testing are discussed in Section II-C. The poles are then cut to a specific length in the longitudinal direction for the longitudinal compression testing. The procedures are detailed in Section II-D. In Section III, the results from the static break test and the compression test are analyzed against the extracted stress wave characteristics. Fig. 1 illustrates the test sequence and the associated correlation analysis.

II. Methodology and Experimental Setup

A. Through-Transmission Mode

The sectional plane above grade is first determined. An arbitrary 0°–180° is chosen as the reference point in this sectional plane, as shown in Fig. 2(a). Two embedded waveguides are inserted 15 mm into the medium. The same procedure is repeated for the 90–270 orientation. These two orientations can produce different responses. This phenomenon is primarily due to the orientation of the local imperfection in the sectional plane with respect to the direction of the traveling stress field. Strong reflection can occur when the lengthwise direction of the imperfection is perpendicular to the propagation direction, causing interference and stronger attenuation at the receiving end. When the lengthwise direction of imperfection is parallel to the propagation direction, the interaction is much weaker. This process is illustrated in Fig. 2(b). Hence, the drastic difference in signals between the two orthogonal directions is an indication of a local imperfection. This study compares the two orientations and selects the highest signal-to-noise (SNR) for the subsequent analysis. When both orientations result in similar energy and temporal responses, it is often an indication of a global response of the sectional plane.

B. Characteristics of Rayleigh Mode Response

An acoustic device, UB1000, produces stress waves here and is designed to generate a narrow-band radiation source of 50 kHz utilizing a high-power piezoelectric transducer. Custom circuitry performs two main functions: 1) to produces high voltage excitation and 2) samples the analog transducer signal and converts it into time-series digital signal using the onboard analog-to-digital converter (ADC) [21]. The device is coupled to an embedded waveguide inserted into the wooden medium to produce radial, and circumferential Rayleigh modes [12].

A previous study by Lee [18] concluded the velocity and diffusive characteristics of the circumferential Rayleigh mode termed *arrival mode number 2* (AW2) can characterize the material properties near the half-space boundary. Lee *et al.* [22] extracted the Rayleigh mode from the complex stress wave response in the circular cross-sectional plane of the groundline region. The study by Shangguan *et al.* [23] indicated that the decay mechanism could contribute to the loss of porosities. Based on Biot's poroelastic formulation, the viscous damping coefficient of the displacement field depends on the coupling factors [24] and [25], which cause amplitude attenuation of the propagating stress wave. The aggregate response of velocity and amplitude inspires the use of an analytic wavelet to represent the temporal waveform

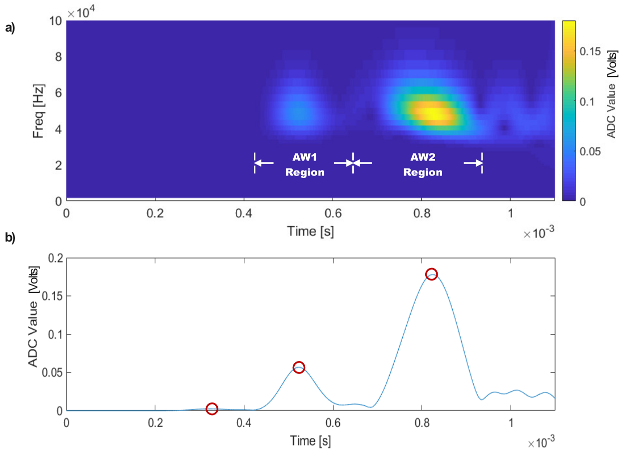

Fig. 3. (a) TF representation of the received ultrasonic signal using wavelet transformation. (b) Energy response in the temporal domain at the ultrasonic excitation frequency.

in the TF domain. The most proper wavelet tends to have a matched shape as the signal in question [26]. Among the examined mother wavelets, the Gabor wavelet exhibits a temporal response similar to the transient waveform estimation by the dual waveguide configuration. It produces an acceptable frequency resolution for spectral analyses in the low-frequency region. The findings from analytical and numerical models [22] show the Gabor continuous wavelet transformation (CWT) produces a desirable temporal and spectral representation of the signal to detect the mechanical and the poroelastic variations in the propagating medium. Fig. 3 depicts TF representation of digitized time-series signal. Two enhanced regions correspond to the energy arrival of AW1 and AW2 arrival regions as illustrated in Fig. 3(a). Extraction of the fundamental frequency of the received waveform yields the energy response in the temporal domain as illustrated in Fig. 3(b). The circled peaks correspond to the arrivals of dominant energy propagation. The peak value provides both temporal information which can translate to the propagation velocity and the energy attenuation.

1) AW2 Average Arrival Velocity: The proposed wavelet analysis technique extracts the temporal-energy response in the signal. By discarding the effect of intermodal interference, the stress-energy of the specific arrival mode dominates the energy contained within the selected arrival region. Hence, this study focuses on the extraction of the peak energy to determine the Rayleigh mode propagation. Since the propagation plane has a dimensional variation based on the pole class and the tapering effect above grade, the average propagating velocity with the corresponding circumference [18] is used at the plane of propagation. That is,

$$\bar{v}_{\mathrm{pe}} = \frac{C_{B,\mathrm{BP}}}{t_{\mathrm{pe}}} \tag{1}$$

where $C_{B,\mathrm{BP}}$ is the circumference of the propagation plane, t_{pe} is the arrival time at the energy peak.

2) Energy Attenuation Coefficient α_{pe}: In linear viscoelastic solids such as wood, the inelastic scattering, and the irreversible process attenuate the wave energy. This process can be explained theoretically by analyzing Biot's poroelastic formulation and the increase of porosity due to incipient decays [12]. To quantify the energy attenuation, peak energy is used to extract the primary mode, and the corresponding attenuation can be obtained using the following power-law model [27]:

$$I(\alpha, x) = I_0 e^{-\alpha x} \tag{2}$$

where I_0 is the initial intensity of the stress wave, I is the energy flux measured in an attenuating medium at a distance x from the source, and α is the attenuation coefficient. The power-law model describes the received energy intensity as a function of the initial wave intensity, propagation distance, and the attenuation coefficient. The attenuation coefficient strongly couples with the property of the medium [12] and provides the means to characterize the condition of the medium. By manipulating (2) and only considering the peak energy attenuation, it yields the expression for peak energy attenuation coefficient α_{pe}

$$\alpha_{\mathrm{pe}} = \frac{2}{C_{B,\mathrm{BP}}} \ln\left|\frac{I_0}{I}\right| \tag{3}$$

where $|\cdot|$ denotes the absolute value, $C_{B,\mathrm{BP}}$ is the circumference of the sectional plane in question. I_0 is a constant. It can be determined by measuring the energy response of a pole at 24 and 48 in above ground line (AGL) (see Table I). The tapering geometry of a pole forms two linearly independent equations for calculating I_0.

TABLE I
SAMPLE SET FOR I_0 DETERMINATION

AGL [inches]	Circumference [inches]	Peak Amplitude of AW2 [volts]
24	47.72	1015
48	46.88	1499

C. Static Break Test

Mechanical testing of wood poles was carried out per the test and data collection requirements of [4]. Fig. 4(b) illustrates the actual setup of the test. A test specimen is restrained at the groundline and few inches above the bottom of the pole to simulate the ground support. A cart shown in Fig. 4(b) helps support the pole to eliminate orthogonal load due to gravity. A tip load is applied 2 ft from the top of a pole using the variable speed winch until reaching the sufficient failure force.

To measure the deflection, a system of four draw-wire sensors measures the pole deflection. Two draw-wire sensors measure the movement 2 ft from the tip at the point of load application. Two draw-wire sensors measure the rotation or ground-line movement at the bottom, allowing the exact measurement of the tip location with respect to the groundline. A load cell shown in Fig. 4(a) is mounted on the speed winch measures half of the applied load.

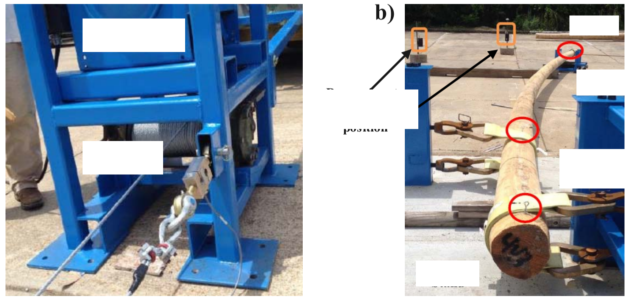

Fig. 4. Setup of the static break test (a) winch is housed in a stable structure mounted to the ground and (b) shows a wooden pole being deflected when a load is produced by the winch via the winch cable.

Based on the measured failure load and the measured deflection, the empirical value of the *maximum fiber strength* at the groundline can be calculated via the following [28] and [3]:

$$F_b = 32\pi^2 P(a - \quad a)/C_a^2 \tag{4}$$

where F_b denotes the maximum fiber stress of the location of the *plane of rupture* (POR), P is the imposed failure tip load, C_a is the circumference of the POR. a is the longitudinal distance between the load point and the break, and a is the maximum longitudinal deflection which is expressed as, $a = \quad_L[1-(b/L)^3]$.

During the test, a test specimen is first rested on a test stand and restrained at the predetermined mounting points. Based on the specimen's pole class, the winch placement or the load point is determined per [4]. Each specimen was tested with the load applied at a constant rate. Simultaneously, the tip position is measured at a 10 Hz sampling rate. After completing the test, the load and deflection measurements are used to determine the modulus of elasticity (MOE) and the modulus of rupture (MOR).

D. Compression Test

Since the rupture plane from the static break test produces an unsuitable surface for the longitudinal compression testing, a 1-ft cylindrical specimen is cut at about one foot from the rupture plane to avoid the alternation of mechanical property. The prepared specimen is stored in a controlled environment with a temperature of 75 °F, relative humility of 50% for 43 days. The compression parallel to the grain procedure was done per [29]. Using 1-in by 1-in square metal rod, the load was applied to the surface of specimens at a rate of 0.1 in/min until 0.1 in indentation is achieved. The load is recorded to calculate the corresponding compression stress. Fig. 5 shows the setup of the experiment. The experiment uses nine different points with five positioned in the heart region and four positioned in the shell region to calculate the average response in both the shell and heart regions of the test surface. The test configuration is shown in Fig. 6.

E. Strength Performance Metrics

The pole structural strength performance is evaluated using the fiber strength at the rupture plane and the overall remaining strength of the pole. Each parameter is described separately below.

Fig. 5. Setup of the compression test.

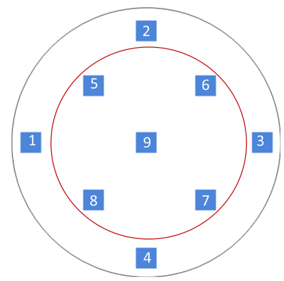

Fig. 6. Locations of nine compression test points on the cross-sectional plane. The red circle is an approximate boundary separating the shell and heart regions.

1) Maximum Fiber Strength and Percentage Remaining Fiber Strength: To normalize the variation of different pole classes, the fiber strength measured at the break point is compared against the designed fiber stress F_d derived from [3]. It is termed the *percentage remaining fiber strength* (% RFS). The mathematical expression is detailed in the following:

$$\%\ \mathrm{RFS} = \frac{F_b}{F_d} \tag{5}$$

where F_b is the measured fiber strength based on (4) and F_d is the designed fiber strength based on Table I in [3]. Since this metric compares the measured strength to the design strength of the specific species, it is a normalization process to estimate the level of the strength degradation.

2) Percentage Remaining Strength: The *percentage remaining strength* (% RS) defined by the following expression:

$$\%\ \mathrm{RS} = \frac{P}{P_d} \tag{6}$$

where P is the load at failure and P_d is the designed class tip load or maximum load capacity. The design class tip bending capacity τ_{cap} is determined via following expression based on the ANSI 05.1 [30]:

$$\tau_{\mathrm{cap}} = P_d L = k F_b C^3 \tag{7}$$

where k is a conversion constant ($k = 0.000264$). F_b is the nominal fiber strength at the ground line, and C is the ground line circumference. L is the distance between the ground line and the load point. Based on the bending capacity, the max load capacity P_d can be obtained. As noted in ANSI O5.1, this calculation contains a *coefficient of variation* (COV) of about 20%.

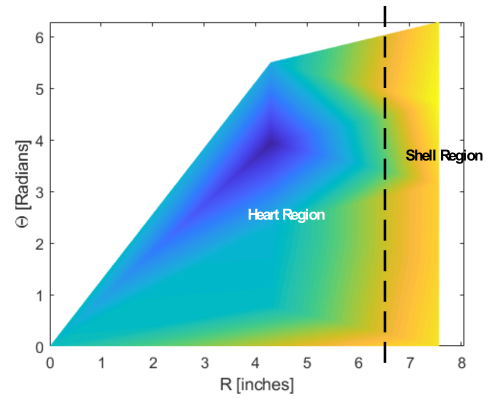

Fig. 7. Result from the linear scattered interpolator, and R denotes the radial direction and θ denotes the tangential direction.

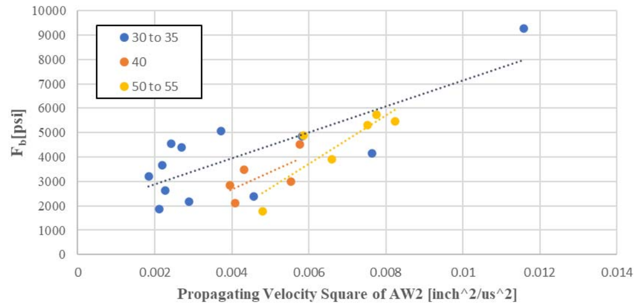

Fig. 8. Average propagation velocity square of AW2 versus the fiber strength at the rupture location.

3) Average Compression Shell Strength: Based on the compression result using the method detailed in Section II-D, the assumed coordinate of the test points and the associated compression values are imported to a scatter interpolator to generate an overall response of the entire specimen. To prevent any unrealistic strength gradients in the overall compression response, the linear interpolator is used to produce a C^0 continuity function resulting in a smooth distribution of compression results in the computational domain. To incorporate the orthotropic property of the cross-sectional plane, the proposed interpolation was performed in the polar coordinate system. The result from one of the specimens is shown in Fig. 7. The ACS strength value is calculated using the RMS defined as

$$x_{\mathrm{RMS}} = \sqrt{\frac{1}{N}\sum_{n=1}^{N}|x_n|^2} \tag{8}$$

where N is the number of data points, x is the compression value obtained from the linear interpolator at the selected shell region.

III. Results and Analysis

A. Model Selection and Correlation Analysis

This section focuses on the justification of the correlation model between the characteristics of the elastic waveform and various mechanical properties determined through the static break test. Based on the formulation produced by Lee [18], the result suggests that the steady-state Rayleigh mode propagation is an aggregate motion of the fast and slow modes associated linearly with the phase velocity of the dilatational and distortional fields, which are expressed as [31]

$$c_L^2 = \frac{\lambda + 2\mu}{\rho}$$
$$c_T^2 = \frac{\mu}{\rho} \tag{9}$$

the above equation suggests a linear relationship between the mechanical property and the velocity square. Henceforth, this model will be used to perform data fitting and correlation analysis.

Prior work conducted by Biot [24] formulated the attenuation coefficient α of the poroelastic wave as a viscous damping term in their governing wave equation. That is,

$$\alpha = \frac{32\mu\beta}{d^2} \tag{10}$$

where μ is the fluid viscosity, β is the porosity, and d is the largest linear dimension of the pores. This expression suggests that the damping coefficient appears linearly with material loss. By combining the viscous damping model with the power model discussed in Section II-B2, the logarithmic model can be assumed to analyze the correlation relationship between the energy attenuation and the mechanical property.

B. Rayleigh Mode (AW2) Response to F_b

Sectional measurements using the UB1000 device are performed prior to the static break test at −12, 0, 12, 24, 36, and 48 in above the ground-line plane. Each cross-sectional measurement is termed the plane of measurement (POM). The AW2 is extracted according to [12], the obtained average velocity and the energy response are compared with the strength performance metrics. After the proposed static break test on the entire sample set is performed, the location of POR is measured. The poles with POR within ±3 in of the POM were selected. This approach assumes minimal property variation in the longitudinal direction.

Twenty-three poles are used in this study due to the close proximity between the POM and POR. Within this sample set, the poles are from a diverse population of different species ranging from 30 to 55 ft. The samples are grouped based on the lengths to analyze if the age of the pole would impact the stress wave characteristics. Based on the prior discussion in Section II-B, the average velocity and the attenuation coefficient are depicted in Figs. 8 and 9. Fig. 8 compares the average propagating velocity square at the POM to the fiber strength at the POR. Using the linear regression model, the three groups 30–35, and 40, and 50–55 exhibit three different correlations with the highest in the 50–55 group. All groups suggest a directly proportional linear correlation between the average velocity and the fiber strength. The average correlation coefficient across all length groups is 0.54.

Fig. 9 compares the peak energy attenuation coefficient α_{pe} against the fiber strength at the POR. The energy response

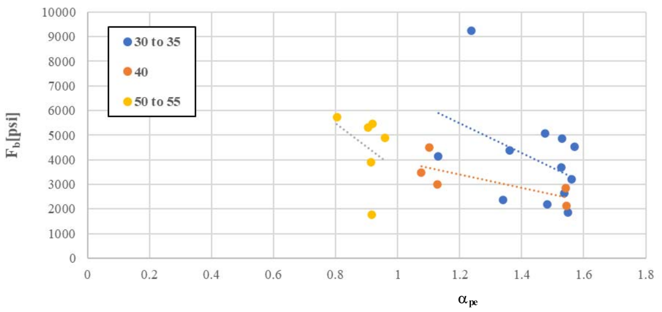

Fig. 9. Peak attenuation coefficient α_{pe} of AW2 versus fiber strength at the rupture location.

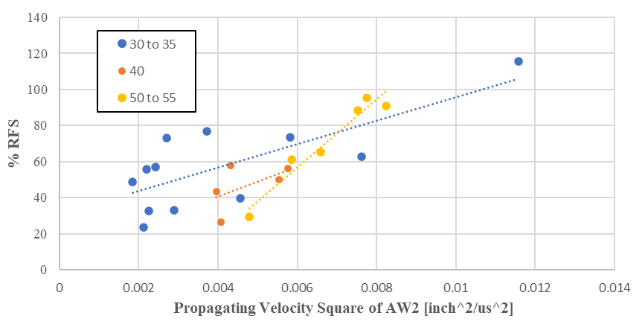

Fig. 10. Average propagation velocity square of AW2 versus the % RFS.

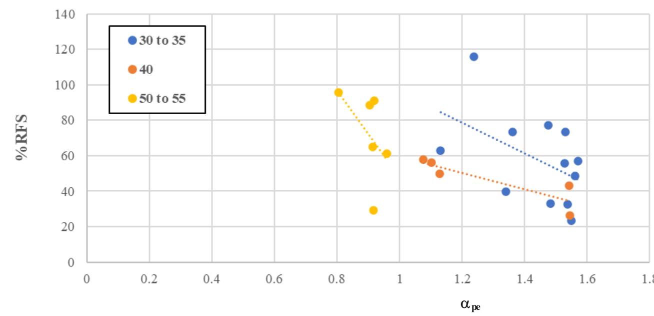

Fig. 11. Peak attenuation coefficient α_{pe} of AW2 versus the % RFS.

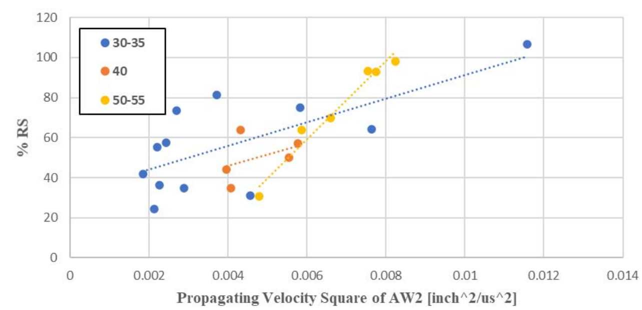

Fig. 12. Average propagation velocity square of AW2 versus % RS.

yields a smaller correlation coefficient compared to the average velocity depicted in Fig. 8. Two distinct clusters are formed among the three different length groups. By eliminating the spatial dependency using the power-law model, the result suggests that the larger class poles with greater groundline circumferences tend to have a smaller attenuation coefficient than the smaller class poles with smaller groundline circumference. This finding is pronounced between the length group 30–35 and the length group 50–55. By discarding the outliers, the fiber strength exhibits an inversely proportional relationship with the attenuation coefficient. This result suggests that wood fiber with a stronger fiber strength tends to have less wave energy attenuation than fiber that exhibits a weaker strength. Across all the length groups, the overall correlation coefficient is 0.1.

C. Rayleigh Mode (AW2) Response to the % RFS

The analyses of the % RFS and AW2 response characteristics are depicted in Figs. 10 and 11. In Fig. 10, the result yields three different correlation values among the length groups. This result indicates a similar finding as Section III-B, suggesting the correlation can be improved by individually considering each length group. The overall correlation coefficient is 0.55, stronger than the fiber strength comparison ($R^2 = 0.54$). As recalled, the % RFS based on (5) reflects the property degradation from the nominal designed strength, making this analysis technique more valuable than the fiber strength comparison.

Fig. 11 shows two distinct clusters. The length group of 50–55 has a relatively lower attenuation coefficient than the length groups of 30–35 and 40. This finding agrees with the finding suggested in Fig. 10. This result indicates that the differences in fibril structure between the different length groups need to be considered. The group-specific correlation coefficients suggest that the % RFS has a higher correlation to the attenuation than the fiber strength. This result yields an overall correlation coefficient of 0.2, a significant increase compared to the average correlation coefficient calculated in Section III-B. The overall inversely proportional relation indicates that the attenuation coefficient increases with decreasing % RFS. It supports the hypothesis that mechanical property degradation has a greater energy attenuation than a healthy wooden medium.

D. Rayleigh Mode (AW2) Response to the % RS

Percentage RS indicates the overall structural integrity at the load point based on the ground-line strength assessment. The results are depicted in Figs. 12 and 13. Fig. 12 compares the propagating velocity against the % RS. The R^2 resulting here indicates a slightly weaker correlation than the analyses comparing the fiber strength and the % RFS. Nevertheless, this result suggests a directly proportional relationship between the average propagating velocity and the % RS and agrees with the analyses in Sections III-B and III-C.

A scatter plot between α_{pe} and % RS is depicted in Fig. 13. It shows a weak correlation and a greater uncertainty between the 30–35 and 50–55 groups. However, group 40 appears to have a stronger correlation. Bear in mind that the five available data points do not warrant statistical significance. Fig. 13 shows two distinct data clusters similar to Figs. 9 and 11

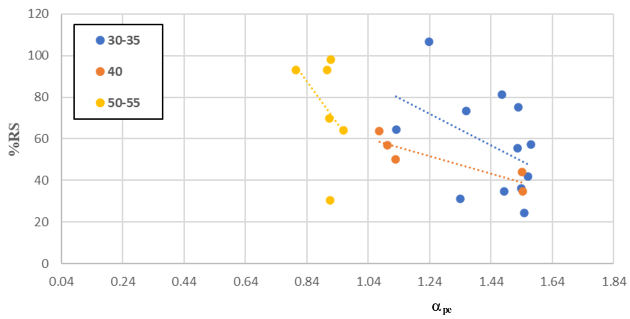

Fig. 13. Peak attenuation coefficient α_{pe} of AW2 versus % RS.

TABLE II
LINEAR AVERAGE CORRELATION COEFFICIENT OF DIFFERENT ANALYSES IN RELATION TO DIFFERENT POLE GROUPS. v AND α_{PE} DENOTE THE AVERAGE PROPAGATION VELOCITY AND THE PEAK ENERGY ATTENUATION COEFFICIENT, RESPECTIVELY

Analysis	30-35	40	50-55	Overall
v^2 - FB	0.62	0.47	0.75	0.54
v^2-%RFS	0.56	0.30	0.94	0.55
v^2-%RS	0.49	0.18	0.96	0.53
α_{pe} - %FB	0.19	0.55	0.11	0.10
α_{pe} - %RFS	0.23	0.76	0.11	0.20
α_{pe} - %RS	0.20	0.79	0.16	0.23

between the 30–40 and 50–55 groups. The overall behavior suggests that the α_{pe} increases with decreasing overall % RS.

E. Correlation Summary

Table II summarizes the correlation coefficients produced from the analyses in Sections III-B–III-D. Using the different analysis techniques, the average propagating velocity of the AW2 appears to have a strong correlation among all three strength performance metrics. The velocity versus fiber strength has the highest correlation in the length groups 30–35 and 50–55, but is relatively weaker in the length group 40. Nevertheless, all three analyses exhibit a similar overall correlation coefficient from 0.53 to 0.55. The energy attenuation versus different strength indicators appears to be much weaker. In length group 40, however, a relatively stronger and distinct correlation of the energy response to all three strength performance metrics.

F. Rayleigh Mode (AW2) Response to the ACS Strength

The section analyzes the compression test results from the procedures detailed in Section II-D and the average compression shell strength using linear scatter interpolator in the polar coordinate domain (Section II-E3). The corresponding AW2 average propagating velocity square and the average compression shell (ACS) strength values are compared in Fig. 14. Using the previous length grouping method, the analysis is repeated three times for the different pole groups (30–35, 40, and 50–55). With the assumed linear regression model, the 30–35 pole group exhibits the highest correlation with the approximate R^2 of 0.37. The correlation performance reduces to 0.22 and nearly 0 for pole groups of 40 and 50–55.

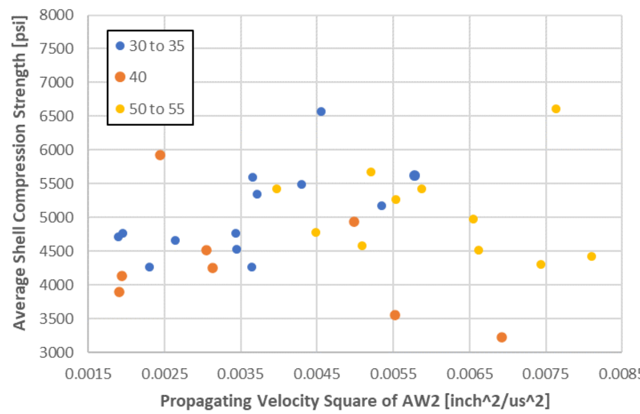

Fig. 14. Correlation between the AW2 velocity square versus ACS values.

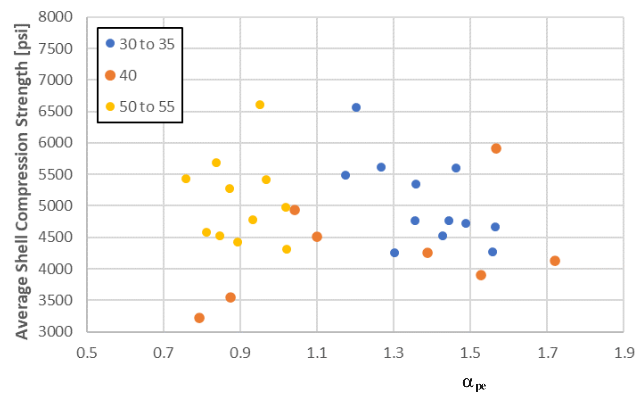

Fig. 15. Peak attenuation coefficient α_{pe} of AW2 versus ACS values.

The strong linear correlation with the directly proportional relation suggests that a greater compression strength in the shell region tends to result in a higher propagating velocity of AW2. This finding is inconsistent in larger pole groups (40 and 50–55), which shows a weaker correlation with different proportional relations.

Using the similar approach as depicted in Fig. 14, the peak energy responses are compared to the different pole groups. Fig. 15 shows the correlation performance of length groups 30–35, 40, and 50–55, respectively. Using the proposed logarithmic linear regression model, the correlation coefficients illustrated a similar finding as shown in Fig. 14 with the 30–35 exhibiting the highest correlation ($R^2 = 0.38$) and the R^2 values decrease with increasing in pole length. The correlation coefficient of group 30–35 indicates an inversely proportional relation, which agrees with the previous finding in Section III-A supporting the conclusion which states that the stress wave tends to have a higher attenuation coefficient in wood with a weaker ACS strength.

Overall, the response of propagating speed and attenuation of AW2 to the ACS strength suggests a correlation if the pole length grouping method is used. A similar study was performed when the species grouping method is used. Using the correlation coefficient as a metric of measurement, the length grouping method has a higher correlation coefficient value than the species grouping method, suggesting a stronger overall dependency on the ultrasonic versus mechanical property correlation for the length group of 30–35. In this study, the moisture content was assumed to be the same after the specimen are exposed to the controlled environment for 43 days. Since the poles were stored horizontally before the tests, the gravitational pull might have contributed to the inhomogeneous distribution of moisture on the POM of each specimen. The proposed linear interpolation function for calculating the ACS values can be improved using a data-driven or physics-based model in future studies.

IV. Conclusion

This study presented a comparative analysis of examining the efficacy of the ultrasonic-based NDT. This work correlated the fiber strength, the percentage remaining fiber strength, and the remaining pole strength resulting from the test with the extracted ultrasonic wave features through the standard static break test and compression testing. The result produces a significant overall correlation of 0.5 between the propagating velocity and the measured pole strength. It resulted in an acceptable correlation level of 0.2 between the peak energy level and the measured pole strength. This data-driven result allows future development of ultrasonic analysis algorithms for the pole strength calculation.

The longitudinal compression test was conducted on the cross section surfaces. Using a linear interpolator, the average shell compression strength values were calculated. The result was compared against the corresponding AW2 characteristics. A stronger correlation appears in the length grouping method with a smaller pole length between 30 and 35 ($R^2 \approx 0.4$). Using other interpolation schemes that are physics-driven and the contribution of moisture can improve the correlation coefficient. More empirical data will improve the statistical confidence and help validate the correlation result. This study reveals the efficacy of the ultrasonic-based NDT for wood pole groundline characterization and contains significant findings for future studies of understanding the correlations at a more fundamental level.

Acknowledgment

Yishi Lee would like to thank the equipment support by the Utility Asset Mangement Inc. Denver, CO, USA, and Dairyland Power Cooperative from La Crosse, WI, USA, to provide the samples of the utility poles used in this study.

References

[1] H. Roliadi, C. Y. Hse, E. T. Choong, and T. F. Shupe, "Decay resistance of out-of-service utility poles as related to the distribution of residual creosote content," *Forest Products J.*, vol. 50, no. 11, pp. 64–68, Nov. 2000.

[2] J. E. Winandy, B. Bernhardt, D. Brooks, A. Sinha, and J. J. Morrell, "Modeling effects of incising on flexural properties of green Douglas fir and western hemlock lumber," *J. Test. Eval.*, vol. 49, no. 6, Nov. 2021, Art. no. 20200308.

[3] *Wood Poles Specifications and Dimensions*, Standard ANSI-O5.1, American National Standards Institute, 2002.

[4] *Standard Test Methods of Static Tests of Wood Poles*, Standard ASTM D1036-99(2017), ASTM International, 2017.

[5] M. G. C. Uzcategui, R. D. Seale, and F. J. N. França, "Physical and mechanical properties of clear wood from red oak and white oak," *BioResources*, vol. 15, no. 3, pp. 4960–4971, May 2020.

[6] E. Fukada, "The vibrational properties of wood I," *J. Phys. Soc. Jpn.*, vol. 5, no. 5, pp. 321–327, 1950.

[7] V. Bucur, "An ultrasonic method for measuring the elastic constants of wood increment cores bored from living trees," *Ultrasonics*, vol. 21, no. 3, pp. 116–126, May 1983.

[8] J. I. Dunlop, "Damping loss in wood at mid kilohertz frequencies," *Wood Sci. Technol.*, vol. 12, no. 1, pp. 49–62, 1978.

[9] H. Suzuki and E. Sasaki, "Effect of grain angle on the ultrasonic velocity of wood," *J. Jpn. Wood Res. Soc.*, vol. 36, no. 2, pp. 103–107, 1990.

[10] C. Senalik, "Detection and assessment of wood decay–glulam beams and wooden utility poles," Ph.D. dissertation, Dept. Elect. Comput. Eng., Univ. Illinois, Champaign, IL, USA, 2013.

[11] R. G. Payton, "Wave fronts in wood," *Quart. J. Mech. Appl. Math.*, vol. 56, no. 4, pp. 527–546, Nov. 2003.

[12] Y. Lee, "Ultrasonic-based condition assessment of wooden utility poles," Ph.D. dissertation, Dept. Ind. Enterprise Syst. Eng., Univ. Denver, Denver, CO, USA, 2020.

[13] J. E. Winandy and J. J. Morrell, "Relationship between incipient decay, strength, and chemical composition of Douglas-fir heartwood," *Wood Fiber Sci.*, vol. 25, no. 3, pp. 278–288, 1993.

[14] V. Bucur and F. Feeney, "Attenuation of ultrasound in solid wood," *Ultrasonics*, vol. 30, no. 2, pp. 76–81, Mar. 1992.

[15] H. Kim and S. W. Heo, "Time-domain calculation of spectral centroid from backscattered ultrasound signals," *IEEE Trans. Ultrason., Ferroelectr., Freq. Control*, vol. 59, no. 6, pp. 1193–1200, Jun. 2012.

[16] R. Prakash, "Non-destructive testing of composites," *Composites*, vol. 11, no. 4, pp. 217–224, Oct. 1980.

[17] M. M. Faraji, S. B. Shouraki, and E. Iranmehr, "Fuzzy based algorithm for acoustic source localization using array of microphones," in *Proc. Iranian Conf. Electr. Eng. (ICEE)*, May 2017, pp. 2102–2105.

[18] Y. Lee, "Diffusive subsurface propagation of Rayleigh mode induced by embedded ultrasonic waveguide," *J. Acoust. Soc. Amer.*, vol. 148, no. 4, p. 2718, 2020.

[19] Y. Lee, M. Mahoor, and W. Hall, "Rayleigh mode excitation at the half-space boundary in wood using embedded elastic waveguides," in *Society of Wood Science and Technology International Convention, Tenaya Lodge*. Yosemite, CA, USA: Society Wood Science Technology, 2019, pp. 212–219.

[20] C. A. Senalik, F. J. N. França, R. D. Seale, R. J. Ross, and R. Shmulsky, "Estimating lumber properties with acoustic-based technologies—Part 2: Ultimate tension stress estimation from time- and frequency-domain parameters," *Wood Fiber Sci.*, vol. 52, no. 4, pp. 390–399, Nov. 2020.

[21] D. Hall, Y. Lee, and W. Hall, "Acoustic probe for inspection of wooden specimen," U.S. Patent 16 518 762, May 21, 2020.

[22] Y. Lee, M. Mahoor, and W. Hall, "A 2D numerical model of ultrasonic wave propagation in wooden utility poles using embedded waveguide excitation technique," *Wood Fiber Sci.*, vol. 52, no. 1, pp. 87–101, Jan. 2020.

[23] W. Shangguan *et al.*, "Cell wall property changes of white rot larch during decay process," *BioResources*, vol. 9, no. 3, pp. 4297–4310, Jun. 2014.

[24] M. A. Biot, "Theory of propagation of elastic waves in a fluid-saturated porous solid. II. Higher frequency range," *J. Acoust. Soc. Amer.*, vol. 28, no. 2, pp. 168–178, Mar. 1956.

[25] Z. E. A. Fellah, M. Fellah, C. Depollier, E. Ogam, and F. G. Mitri, "Wave propagation in porous materials," in *Computational and Experimental Studies of Acoustic Waves*. London, U.K.: InTech, 2018, pp. 99–119.

[26] W. K. Ngui, M. S. Leong, L. M. Hee, and A. M. Abdelrhman, "Wavelet analysis: Mother wavelet selection methods," in *Applied Mechanics and Materials*, vol. 393. Stafa-Zurich, Switzerland: Trans Tech, 2013, pp. 953–958.

[27] V. Bucur and I. Böhnke, "Factors affecting ultrasonic measurements in solid wood," *Ultrasonics*, vol. 32, no. 5, pp. 385–390, Sep. 1994.

[28] P. Bajpai, "Biermann's handbook of pulp and paper," in *Raw Material and Pulp Making*, vol. 1. Amsterdam, The Netherlands: Elsevier, 2018.

[29] *Standard Test Methods for Small Clear Specimens of Timber*, Standard ASTM D143-21, May 2021.

[30] R. W. Wolfe and R. C. Moody, "Ansi pole standards: Development and maintenance," in *Proc. 1st Southeastern Pole Conf.*, Madison, WI, USA, 1994, pp. 143–149.

[31] J. L. Rose, *Ultrasonic Waves in Solid Media*. Oak Park, IL, USA: ASA, 2004.

Yishi Lee received the B.S. and M.S. degrees in physics from Embry–Riddle Aeronautical University, Daytona Beach, FL, USA, in 2007 and 2013, respectively, and the Ph.D. degree in mechatronic engineering from the University of Denver, Denver, CO, USA, in 2020. He is currently an Assistant Professor with the Engineering and Engineering Technology Department, Metropolitan State University of Denver, Denver, CO, USA. He is also working with an industry partner specializing in ultrasonic-based stress waves for nondestructive evaluation in wooden utility poles, leading the firm in research and development and algorithmic developments. The resultant features are used for condition characterization and advance the NDE technology. His collaborative efforts with multiple government agencies, academic institutions, and private firms have helped produced numerous journal articles, conference papers, and patents. His research focuses on advancing the applications of ultrasonic signal processing and analysis based on physical principles.

Frederico José Nistal França received the Wood Industry Engineering degree and the master's degree in forest science from the Federal University of Espírito Santo, Espírito Santo, Brazil, in 2012 and 2014, respectively, and the Ph.D. degree in sustainable bioproducts from Mississippi State University, Starkville, MS, USA, in 2017.

He is an Assistant Research Professor at Mississippi State University. His areas of interest are physical and mechanical properties of wood, nondestructive evaluation of wood (NDT), modeling, heat, and mass transfer during wood drying and he is currently investigating advanced vibrational measurements as an indicator of lumber strength.

R. Daniel Seale received the degree from Mississippi State University, Starkville, MS, USA, and the Ph.D. degree in applied economics from Clemson University, Clemson, SC, USA, in 1983.

He is a James R. Moreton Fellow and a Thompson Professor with the Department of Sustainable Bioproducts, Mississippi State University. Since joining the Staff with the Department of Forest Products in 1983, he has worked with many industry segments including plywood, particleboard, and oriented strand board (OSB), solid lumber including hardwood and softwood, poles, and pilings, and the furniture industry. He manages the mechanical testing and pressing facilities of the department. A recent project involving Dr. Seale, Dr. Fred Franca, and Songi May Han led to the development of an IPhone application called "Smart Thumper" that is the first nondestructive evaluation of wood (NDT) tool that is available to consumers and capable of testing lumber utilizing longitudinal vibration and/or transverse vibration. His research areas include economics, manufacturing composite wood products, product mix for plywood and OSB, and database applications tailored to individual manufacturing companies.

Jerrold E. Winandy started his own consulting firm specializing in forensic wood science, wood durability, and bio-resource sustainability in 2008. He has been an Adjunct Professor of wood science and engineering at the University of Minnesota, Minneapolis, MN, USA, since 1998. Prior to 2008, he served for over 30 years as a Research Wood Scientist with Engineering Properties of Wood and later as the Project Leader of the Engineered Composites Science Research Units both located at the USDA Forest Products Laboratory, Madison, WI, USA. He has authored/coauthored over 200 technical publications and holds two patents. His research on the very early stages of thermochemical degradation and biological decay has provided insight into how changes in the chemical composition of the wood cause significant reductions in the engineering properties of wood and bio-based composites.

Christopher A. Senalik received the B.S. and M.S. degrees in general engineering and the Ph.D. degree in systems and entrepreneurial engineering from the University of Illinois Urbana–Champaign, Champaign, IL, USA, with a focus on non-destructive testing and evaluation, in 1997, 2001, and 2013, respectively.

He is currently a Research General Engineer with the Forest Products Laboratory, Madison, WI, USA, where he develops methods of NDE for wood-based products using acoustics, stress waves, and radar.